# Development and Characterization of Polypyrrole-Polylactide Conductive Open-Porous Composites

**Christine Chan, Hani E. Naguib**

*Department of Mechanical and Industrial Engineering, University of Toronto, Toronto M5S 3G8, Canada*

Received 27 October 2009; accepted 30 January 2010
DOI 10.1002/app.32197
Published online 3 May 2010 in Wiley InterScience (www.interscience.wiley.com).

**ABSTRACT:** In this study, conductive porous composites were fabricated using the host substrate with an interconnected porous network, followed by the penetration and deposition of polypyrrole (PPy) to create a continuous conductive network. The open-porous host substrate was processed using polylactide (PLA) with compression molding and salt leaching techniques. Three different salt contents were varied from 75 wt %, 85 wt %, and 90 wt %, which were referred to by their salt-to-polymer mass ratios of 3, 6, and 9, respectively. The porous network was made conductive by coating its interior surfaces through *in situ* polymerization of PPy using iron (III) chloride as the oxidant species. These porous composites were then characterized to analyze the relationships between their morphology and their physical, conductive, and mechanical properties. The mechanical properties were then fitted with numerically simulated results from finite element modeling (FEM). © 2010 Wiley Periodicals, Inc. J Appl Polym Sci 117: 3187–3195, 2010

**Key words:** conducting polymers; polypyrroles; porous; modulus; coatings

## INTRODUCTION

Conducting polymers are unique materials that have generated much research interest because of their intrinsic conductive properties. In contrast, conducting polymers are typically very brittle with poor mechanical properties and processability. These shortcomings can be improved by combining the conducting polymer with a host polymer to form composites. In that way, these composites can benefit from the electrical properties of the conducting polymer as well as the processability and mechanical properties of the host polymer. Composites can be prepared by dispersing particles of conducting polymer into an insulating host polymer matrix. However, studies have found that the dispersion technique encountered aggregation problems with the conducting particles due to a mismatch of surface tensions and interfacial energy.[1] In addition, a model developed by Scher et al.[2] demonstrated that a minimum of 16–17 vol % of conducting polymer was required to reach the percolation threshold for conductivity. In general, it was found that dispersion of the conductive component within a host material was not an efficient process due to its nonuniform distribution, which highly affects the conductivity of the composites.

Alternatively, composites can also be prepared by *in situ* polymerization of the conducting polymer within a host polymer.[3–5] *In situ* polymerization involves the oxidation and polymerization of the monomer using an oxidant species. One of the most extensively studied conducting polymers is polypyrrole (PPy) because the monomer is easily oxidized, water soluble, and commercially available. The most commonly used oxidant species of ferric salt is iron (III) chloride ($FeCl_3$), which is easily handled and dissolved, and can obtain a highly conductive polymer.[6] Chen et al. found that most conducting materials were achieved when the oxidant-to-monomer ratio was $\sim 2 : 1$.[7] Increasing the pyrrole monomer concentration leads to higher conductivity values for the polymer. As the pyrrole concentration increased, it decreased the polarization of polymerization of pyrrole, as reported by Hwang et al.[8] Lower polarization levels lead to higher conjugation or higher doping in the polymer backbone, which increases the conductivity. Pini et al. demonstrated a drastic increase in conductivity, when the pyrrole concentration increased from 0.1 to 0.3*M*, followed by a slower increase from 0.3 to 0.8*M*, then a drastic decrease in conductivity above 0.8*M*.[9] As an oxidant-to-monomer ratio of 2 : 1 yielded the highest conductivity, optimal concentrations of 0.3*M* pyrrole and 0.6*M* $FeCl_3$ were chosen for this study. *In situ* polymerization has been studied by several groups,

*Correspondence to:* H. E. Naguib (naguib@mie.utoronto.ca).

Contract grant sponsors: Natural Science and Engineering Research Council of Canada (NSERC), Canada Research Chair (CRC), Canada Foundation of Innovation (CFI).

which have polymerized PPy on various host polymers, such as poly(vinyl chloride),[10] poly(vinyl alcohol),[11] and polyurethane.[12,13]

However, there has not been any previous research conducted that utilizes *in situ* polymerization of PPy using polylactic acid (PLA) as the host polymer. PLA is a promising material that has gained increasing popularity over recent years. PLA is a biodegradable and biocompatible polymer that is produced from renewable resources, such as starch and corn. It is a thermoplastic, which allows it to be processed to any desired shape. It also has good mechanical properties, which makes PLA an ideal component for biodegradable materials in packaging, structural, environmental, pharmaceutical, and biomedical applications.[14,15]

The host substrate used for *in situ* polymerization can be porous or solid. Porous substrates may have mechanical advantages over solid bulk substrates. As conducting polymers are usually stiff and brittle, incorporating them into a solid host polymer often embrittles it. However, for a porous substrate, the conducting polymer stiffens the struts of the pore structure, while the composite remains pliable and the modulus of the composite can be controlled to some extent by varying the relative density.[12] In addition, an open-porous structure may improve the efficiency of *in situ* polymerization by facilitating the diffusion of the monomer and oxidant into the host polymer matrix due to its greater surface area. Ruckenstein et al.[16,17] found that the uniform distribution of the conducting polymer with sufficient loading within an insulating porous matrix allowed for the percolation threshold to be reached.

One of the most common ways to create porous structures is particulate leaching with a shaping method, such as casting,[18] extrusion,[19] and compression molding.[20–23] Several studies have been conducted to analyze the effect of processing on the porous scaffolds using particulate leaching with compression molding, using salt as the particulate. Hou et al. found that resultant porous scaffolds remained intact only when the size range of the polymer particles was smaller or equal to the size of the salt particles.[24] Otherwise, the scaffolds were damaged during the salt leaching process and broke into several pieces. Studies have found that the salt particles could not be fully extracted if the salt contents were below 60 wt % or 70 wt % although salt contents over 90 wt % were prone to disintegration.[24,25]

This study describes the fabrication and characterization of open-porous conductive composites. Open-porous substrates were processed using PLA, compression molding, and salt leaching techniques. Three different salt contents were varied from 75 wt %, 85 wt %, and 90 wt %, which will be referred to by their salt-to-polymer mass ratios of 3, 6, and 9, respectively. The porous substrates were made conductive through *in situ* polymerization of PPy using iron (III) chloride as the oxidant species. Characterization of these porous composites was conducted with respect to their physical, electrical, and mechanical properties.

## EXPERIMENTAL

### Materials

PLA pellets (grade 3001D, Natureworks) and sodium chloride particles (Fisher Scientific) were used to fabricate the open-porous network. PLA is a semicrystalline biodegradable polymer with a density of 1.24 g/cm$^3$ and a melting temperature of ~173–177°C, as provided by the supplier. The monomer and oxidant used for the *in situ* polymerization of PPy were aqueous solutions of pyrrole (reagent grade, 98%, Sigma-Aldrich) and iron (III) chloride (reagent grade, 97%, Sigma-Aldrich), respectively.

### Fabrication of composites

#### Fabrication of open-porous substrates

PLA pellets were ground into a fine powder using a 6850 Freezer/Mill (SPEX CertiPrep Group) and sieved to ensure that the particle size was between 54 and 106 μm in diameter. The particle size range of the sodium chloride was 106–250 μm. The PLA and sodium chloride particles were dry blended at different salt-to-polymer mass ratios of 3, 6, and 9. The mixture was then loaded in a circular die and initially compressed at a pressure of 4 tons for 30 s to obtain a solid disc ~12.8 mm diameter. The solid discs were then placed in a circular mold in a heated compression mold at 185°C. The heated plates were positioned to be in contact with the discs for 5 min to melt the PLA, and then a pressure of 1.5 tons was applied to the mold for an additional 10 min to compact and form the disc. The solid discs were then removed from the mold and quenched in ice water. The discs were submerged in distilled water for 48 h with the water changed approximately every 12 h to leach out all the salt particles, resulting in an open-porous PLA substrate.

#### Fabrication of open-porous conductive composites

Solutions of 0.3*M* pyrrole and 0.6*M* iron (III) chloride were prepared for *in situ* polymerization of PPy on the porous PLA substrates. The porous substrates were submerged in the pyrrole solution for 1 h and then immediately transferred to the iron (III) chloride solution for an additional hour. The PPy-coated substrates were then rinsed with distilled water to remove any unreacted and by-products, and dried

overnight in a vacuum chamber to result in the open-porous conductive composite.

### Characterization of composites

#### Optical properties

FTIR-ATR spectra were recorded using an infrared spectrometer (Spectrum 1000, Perkin Elmer) to observe the characteristics peaks of PPy on the PLA substrates. The spectrum recorded in the frequency range from 2000 to 600 $cm^{-1}$.

#### Physical properties

The morphology of the cross sections and surfaces of the composites was observed and analyzed using a scanning electron microscope (SEM JSM-6060). The open-porous samples were characterized by their physical morphology, which included properties, such as relative density, open porosity, pore size, and pore density.

Relative density, $\rho_r$, was calculated as the ratio of the density of the open-porous disc, $\rho^*$, to the density of the solid material, $\rho$, as defined in eq. (1). The density of the open-porous disc was measured as the mass over the total disc volume. The volume of the disc was calculated by the average of three thickness ($t$) and diameter ($D$) measurements as defined in eq. (2).

$$\text{Relative Density}(\rho_r) = \frac{\rho^*}{\rho} \tag{1}$$

$$V_{\text{total}} = t\left(\frac{D^2}{4}\right)\pi \tag{2}$$

Open porosity was calculated as the ratio of open-porous volume within the total disc volume, as defined in eq. (3), where $V_{\text{open}}$ was the volume of the open pores measured from the gas pycnometer (Quantachrome Ultrapyc 1200e) and $V_{\text{total}}$ was the total outer disc volume, as calculated in eq. (2).

$$\text{Porosity}_{\text{measured}}(\%) = \left(1 - \frac{V_{\text{open}}}{V_{\text{total}}}\right) \times 100\% \tag{3}$$

The measured open porosity results were compared with the theoretical open porosity values, which were calculated as the volume fraction of salt within the total volume of salt and PLA before dry blending, as described in eq. (4).

$$\text{Porosity}_{\text{theoretical}}(\%) = \frac{\frac{m_{\text{NaCl}}}{\rho_{\text{NaCl}}}}{\frac{m_{\text{NaCl}}}{\rho_{\text{NaCl}}} + \frac{m_{\text{PLA}}}{\rho_{\text{PLA}}}} \times 100\% \tag{4}$$

The pore morphology of the samples was analyzed using SEM micrographs to characterize the average pore size and pore density. The micrographs were analyzed using ImageJ software, where the pore size was the average diameter of the pores and pore density was defined in eq. (5), where $N$ was the number of pores observed in a given two-dimensional area, $A$.

$$\text{Pore Density}\left(\frac{\#\text{ pores}}{\text{cm}^3}\right) = \left(\frac{N}{A}\right)^{\frac{3}{2}} \tag{5}$$

#### Electrical properties

The conductivity of the composites was obtained using a dielectric/impedance analyzer (Alpha-N Novocontrol Technologies). The conductivity was measured through a frequency sweep of $10^{-2}$–$10^5$ Hz with an applied AC voltage of 1 V. The reported conductivity values were reported at a frequency of 10 Hz for comparison purposes.

#### Mechanical properties

The mechanical properties of the composites were analyzed in terms of the elastic modulus, which was measured from the linear elastic region of the stress-strain curves. The curves were obtained using compression testing (Instron 4465) with a load cell of 5 kN and strain rate of 1 mm/min. The average of three test samples was taken.

## RESULTS AND DISCUSSION

### Morphology

#### Morphology of open-porous structures

The SEM micrographs of the cross sections of the samples were displayed in Figure 1. The unleached, solid samples were shown in Figure 1(a–c) for the 3, 6, and 9 salt-to-polymer mass ratios, respectively. The cross sections demonstrated the compacted solid structures of salt and polymer. Figure 1(d–f) portrayed the cross sections of the porous samples after salt leaching. These porous samples comprised of a network of pores, which resulted from the dissolution of the incorporated salt particles during salt leaching. It was observed that the network of pores transitioned from a distinct structure with well-defined pore walls to a fused arrangement with broken pore walls as the salt-to-polymer mass ratio increased. Higher ratios implied a higher salt content, but lower polymer content. When there were fewer polymer particles to fuse around the salt particles, the resulting pore walls were relatively smaller in thickness, which allowed the walls to be more easily penetrated and broken during salt leaching. On the other hand, a lower ratio

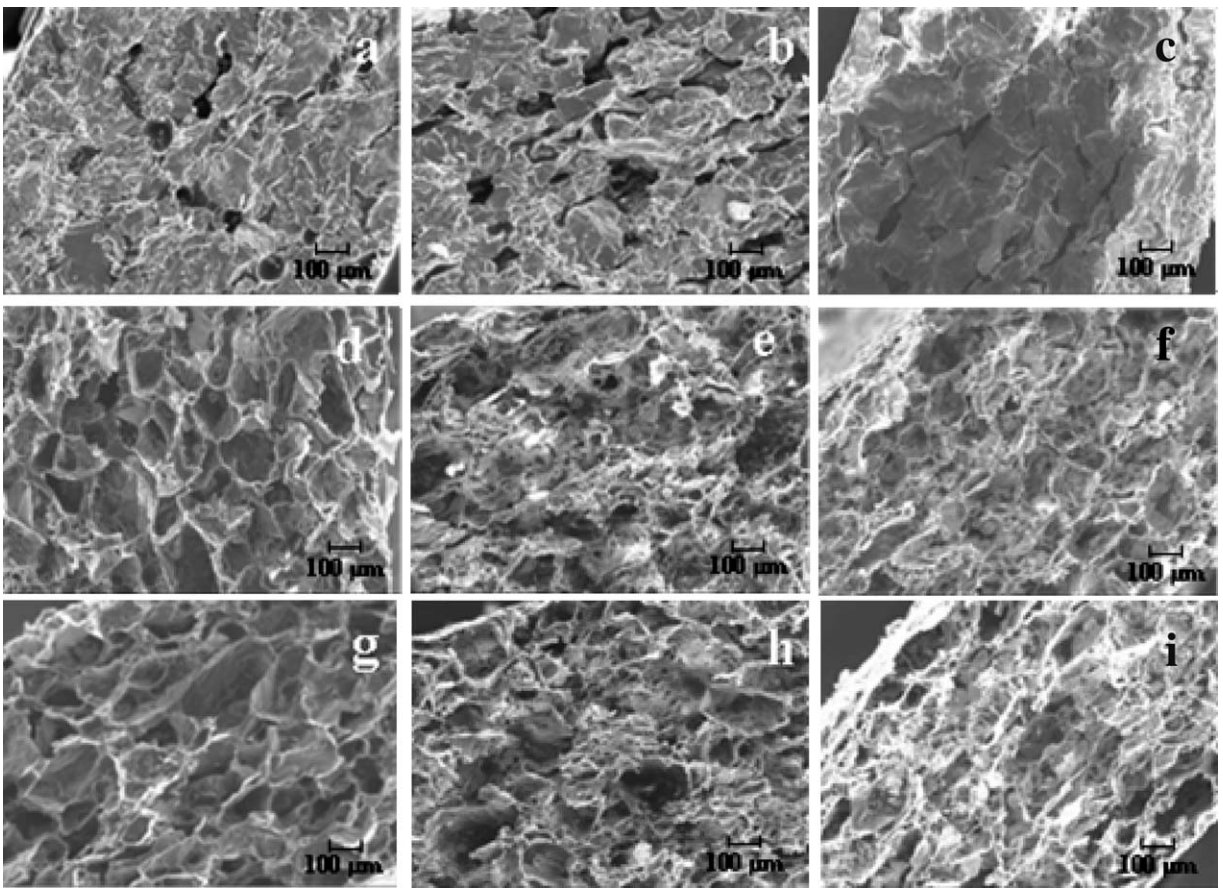


**Figure 1** SEM micrographs of the cross sections of solid (a–c) and porous samples—uncoated (d–f) and coated (g–i).

consisted of a greater polymer content to form thicker walls around the pores for a well-defined pore structure. In addition, Figure 1(g–i) demonstrated the cross sections of the porous substrates, which were subsequently coated with PPy through *in situ* polymerization. It was observed that the PPy coating did not affect the structure of the pore network.

## Morphology of PPy coating

Although the effect of PPy coating on the pore structure was negligible, the presence of PPy on the surface of the samples was characteristically evident under higher magnification as shown in Figure 2. The observed nodular structure of PPy coincided with previous studies, which have also reported

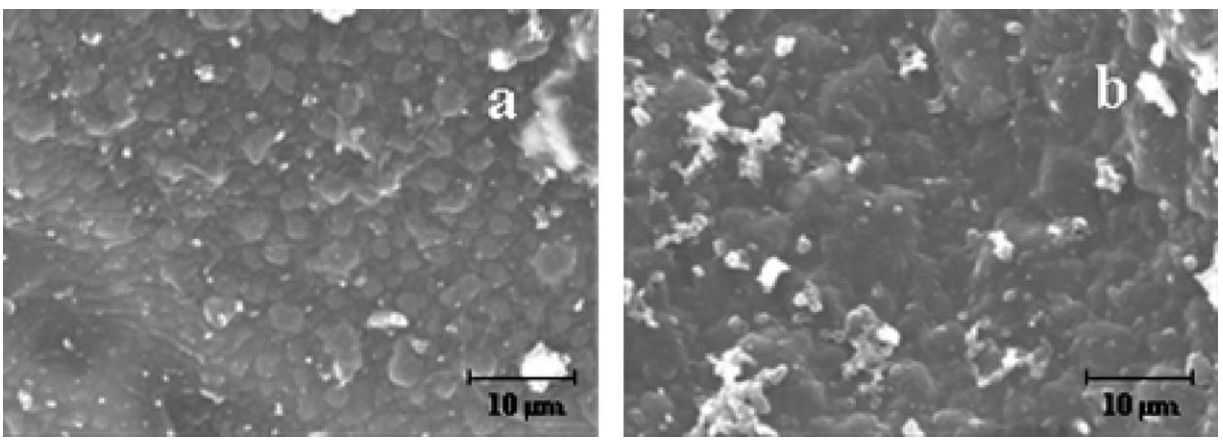


**Figure 2** Polypyrrole nodules on composites fabricated with (a) 3 and (b) 9 mass ratios.

homogeneous distributions of nodules.[26–28] It was also interesting to observe that the nodular structure was different between various salt-to-polymer mass ratios. The 3 mass ratio composite in Figure 2(a) had smaller individual nodules whereas the 9 mass ratio composite in Figure 2(b) had nodules that joined together to form relatively larger nodules. The low salt-to-polymer mass ratio of 3 had a lower salt content and thus lower pore content and surface area for the PPy to deposit on compared with the high mass ratio of 9. As the 9 mass ratio had a higher surface area, it was believed that there was more PPy deposited, leading to the overlap and coalescence of PPy nodules.

## Optical properties

The deposition of PPy inside the PLA substrate was confirmed by infrared spectroscopy (FTIR-ATR), as shown in Figure 3. The peaks observed correspond to the characteristic vibrations associated with PPy.[29–31] It was noted that the characteristic carbon double bond present in PPy was observed at 1548 $cm^{-1}$, which was not observed for PLA.

## Physical properties

### Relative density

As the salt-to-polymer mass ratio increased, it was found that the relative density decreased, as shown in Figure 4. The relative densities of the uncoated substrates decreased from 0.36 to 0.21 to 0.15 as the mass ratio increased from 3 to 6 to 9, respectively. Higher mass ratios indicated a high salt content, which resulted in a larger pore content and void space within the same substrate volume. Therefore, a lower relative density was observed with respect to the solid sample when the salt-to-polymer mass ratio increased. It was also found that the PPy coating on the surface of the substrates did not have an effect on the relative density. The relative densities of the coated porous composites were 0.31, 0.19, and 0.16 for mass ratios of 3, 6, and 9, respectively.

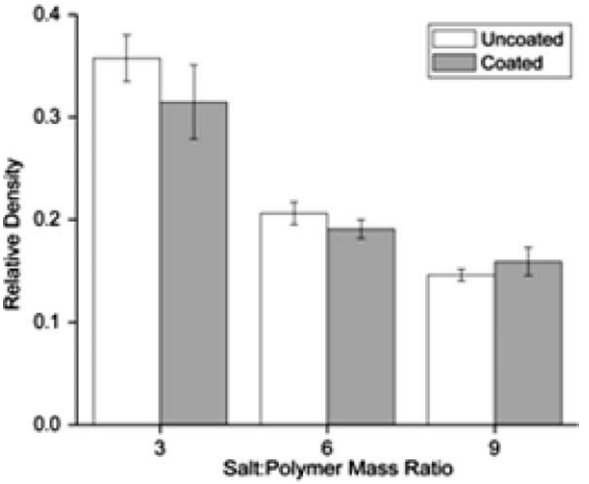


**Figure 4** Comparison of the relative densities for uncoated and coated samples.

### Open porosity

It was found that the open porosity increased as the salt-to-polymer mass ratio increased, as shown in Figure 5. As there were more salt particles compacted in the samples with the higher mass ratios, the neighboring particles were closer together with less polymer fused around them. After salt leaching, the neighboring pores were correspondingly closer with thinner pore walls that were easily broken to

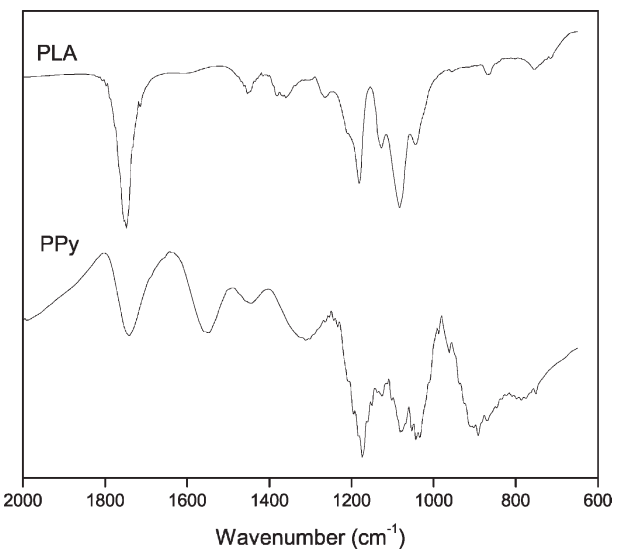


**Figure 3** FTIR-ATR spectra of PLA and PPy.

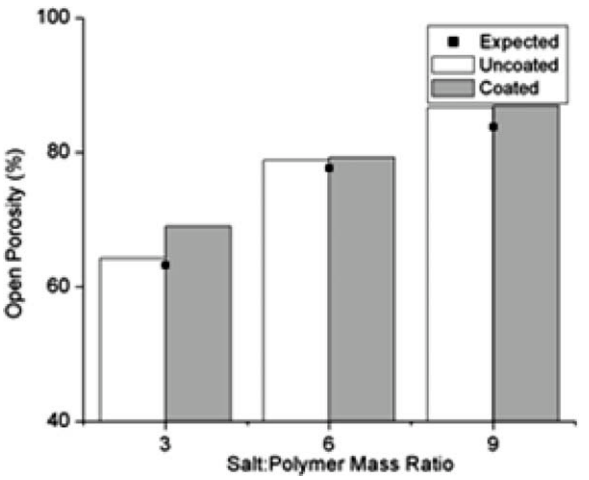


**Figure 5** Comparison of the open porosity values for uncoated and coated samples.

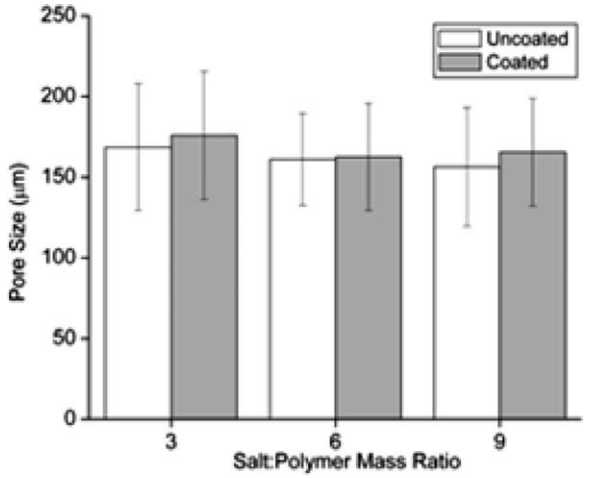


**Figure 6** Comparison of the average pore sizes for uncoated and coated samples.

form an open-pore network. Therefore, the open porosity of the leached, but uncoated substrates increased from 64.3% to 78.8% to 86.6% as the salt-to-polymer mass ratio increased from 3 to 6 to 9, respectively. On the other hand, the values for open porosity of the coated substrates were 69.0, 79.2, and 86.9% for mass ratios of 3, 6, and 9, respectively. It was found that the effect of PPy coating was negligible at mass ratios of 6 and 9, but had a pronounced effect at the lower mass ratio of 3. At the mass ratio of 3, the open porosity increased by 4.7%. This increase was suggested to be due to slight degradation of the pore walls during *in situ* polymerization of PPy. As previously discussed, the pores in the samples fabricated with the 3 mass ratio were relatively more distinct with thicker pore walls, and thus, did not significantly contribute to the interconnected network of pores. However, after immersion in two different aqueous solutions during *in situ* polymerization, the thick-structured pore walls were slightly degraded to open and connect the pores, which led to the relative increase in open porosity. The effect of degradation of the pore walls was less pronounced for the mass ratios of 6 and 9 because those samples have higher surface areas, which provided more regions for PPy coating as opposed to degradation. It was also important to note that the experimental results generally corresponded with the expected values. As the expected values were calculated based on the amount of salt leached out, these theoretical values only considered the open porosity to be the void space occupied by the volume of the salt particles. On the other hand, the experimental results considered the coalescence of pores through broken pore walls in addition to the void space from the salt particles, which resulted in slightly higher values for open porosity.

### Average pore size and pore density

The pore morphology was quantified with measures of average pore size and pore density. It was found that the pore size remained relatively constant as the salt-to-polymer mass ratio was varied, as portrayed in Figure 6. The average pore size ranged from ~156 to 175 μm, which corresponded with the size range of the incorporated salt particles, which was 106–250 μm. Therefore, the size of the pores can be controlled by the size of the salt particles through salt leaching. Figure 7 found that the pore density did not exhibit any significant trends as the salt-to-polymer mass ratio increased. It was expected that the pore density should generally increase with increasing mass ratio as there would be more salt particles leached out. However, a higher salt content would also result in thinner and broken pore walls to allow the coalescence of pores to form larger pores within the same volume, which would counteract the trend and decrease the pore density. Therefore, there were no significant trends found for pore density when the salt-to-polymer mass ratio was varied.

## Electrical properties

Figure 8 demonstrated the conductivity through a frequency sweep. It was observed that the conductivity increased with increasing frequency for the neat PLA while the ppy-coated samples were frequency independent. For neat PLA, the AC conductivity increased from $10^{-14}$ to $10^{-7}$ S/cm as the frequency increased because of the additional tunneling of charge carriers between isolated polymer sites at higher frequencies. On the other hand, the coated samples were shown to be independent of frequency, which indicated that a continuous

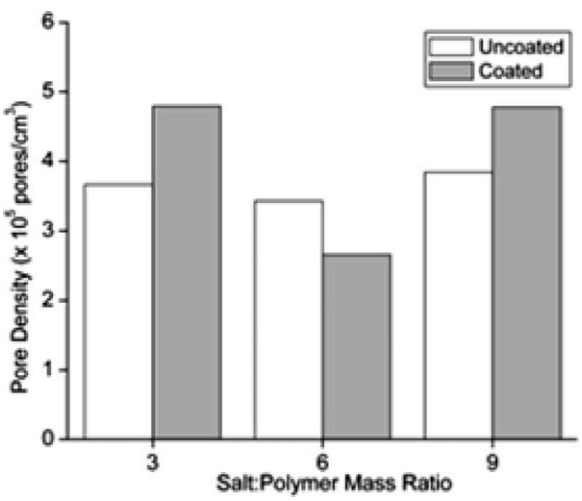


**Figure 7** Comparison of the pore densities for uncoated and coated samples.

conductive pathway of PPy was successfully incorporated within the host substrate to allow for the mobility of charge carriers along the percolation network. The effect of coating the neat PLA porous substrates with PPy increased the conductivity by 6–7 orders of magnitude. The conductivity also increased from $2.24 \times 10^{-4}$ to $9.70 \times 10^{-4}$ to $1.73 \times 10^{-3}$ S/cm as the salt ratio increased from 3 to 6 to 9, respectively. Increasing mass ratios corresponded with a higher open porosity and pore interconnectivity which provided additional surface area for the coating of PPy. Therefore, it was found that the conductivity of the composites can be controlled by varying the porosity, which is determined by the initial salt content during the processing.

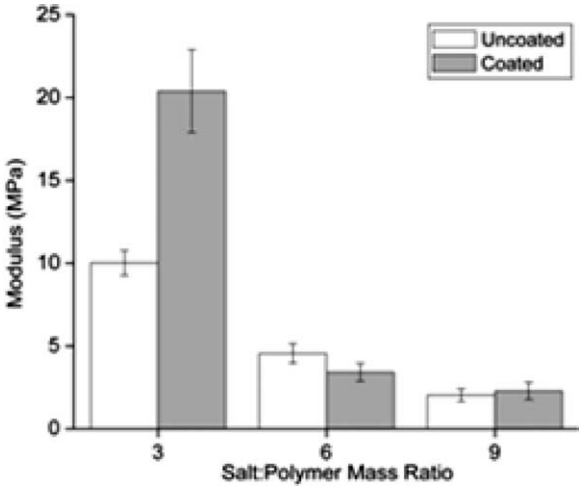


**Figure 9** Comparison of the modulus values for uncoated and coated samples.

### Mechanical properties

The trends for compressive modulus of the porous substrates were displayed in terms of salt-to-polymer mass ratio and relative density. Figure 9 displayed the decreasing trend of modulus when the salt-to-polymer mass ratio increased. As previously discussed, increasing the salt content resulted in a less-defined pore structure with broken pore walls, which produced a lower modulus in comparison with a well-defined pore structure with thicker pore walls. During compression, when the pore walls were already thin and broken, the deformation mechanism of pore wall bending occurred more readily to result in lower mechanical properties. It was also observed that there was not a significant difference in the modulus values between the uncoated and coated samples with the exception of the 3 salt-to-polymer mass ratio composite. The average modulus values of the uncoated substrates were 10.02, 4.55, and 2.03 MPa while the coated composites were 20.38, 3.41, and 2.28 MPa for the mass ratios of 3, 6, and 9, respectively. For the 3 mass ratio sample, the modulus increased 142% after coating it with PPy. This significant increase in elastic modulus was attributed to the stiffening of the struts of the pore walls because of the PPy coating. This effect was not identified in the composites fabricated with higher salt contents because the thin and broken pore walls were not enough to effectively retain a coherent coating of PPy. To elucidate this stiffening effect, Figure 10 established the relationship between modulus and relative density. There was a general squarely proportional trend between elastic modulus and relative density. Interestingly, there was an outlier to this trend which was the coated composite fabricated with the 3 mass ratio. Therefore, it was found that coating the porous substrate with PPy can increase the modulus without increasing the relative density at the same ratio.

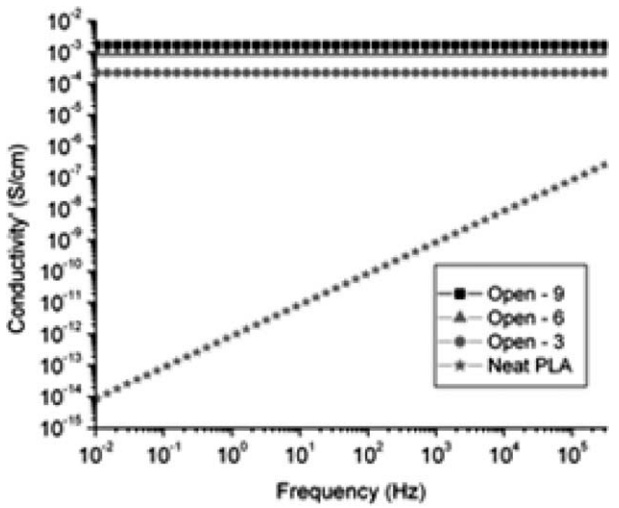


**Figure 8** Conductivity of the open-porous composites as a function of frequency.

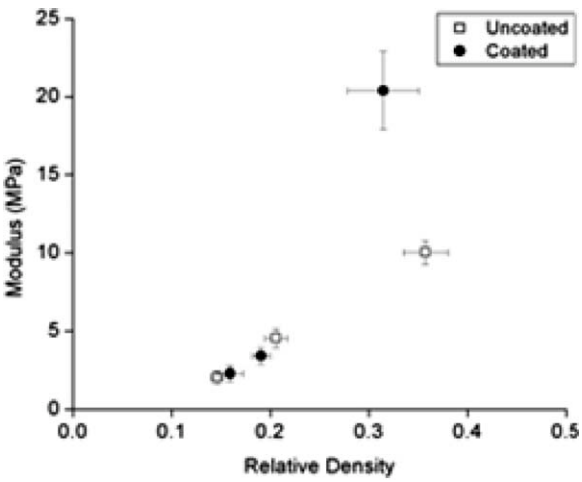


**Figure 10** Modulus as a function of relative density.

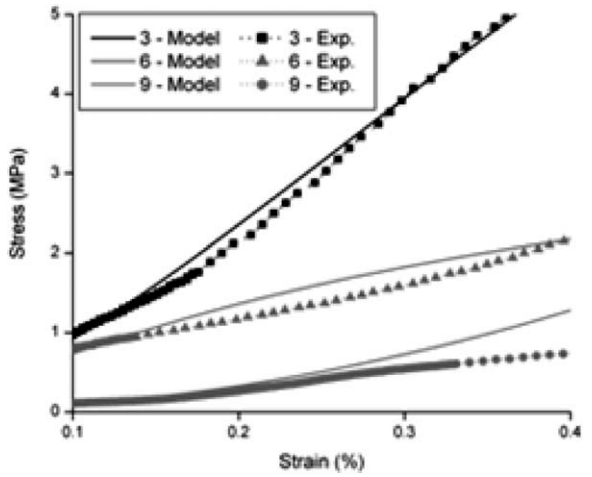


**Figure 11** Comparison of the model and the experimental results for open-porous structures.

Further investigation is needed to fully understand and optimize this stiffening effect.

## FINITE ELEMENT MODELING

The computer software used for FEM was LS-DYNA, which was developed by Livermore Software Technology Corporation. FEM is used to simulate compression testing of the porous host substrates as there are currently no specific models for open-porous PLA materials. The simulated stress-strain curves and elastic modulus values were compared with the experimental data. Optimized model parameters were developed to accurately fit the empirical results. Development of the model with a detailed description of the parameters and characteristics is presented, followed by the analysis parameters at which the results are generated from.

### Model description

Modeling of the compression testing of porous substrates comprised of two identical compression plates with the substrate in between the plates. The physical description of the model was described in terms of the development of the mesh and the material models. The mesh of the compression plates was modeled as a solid box while the substrate was modeled as a solid cylinder. The number of elements in the compression plates was optimized for a mesh size of 15 $\times$ 15, while there were 40 elements for the substrate in the thickness direction. With these optimal mesh parameters defined for the compression plates and substrate, the materials of these components were then identified. For the compression plates, a rigid material model was used because it was assumed that there were no deformations occurring in the plates. The selected material for the plates was steel in which the corresponding density, elastic modulus, and Poisson's Ratio were inputted. For the substrate, a low density foam model was used where the density, elastic modulus, and the stress-strain curve of the porous substrate were inputted.

### Analysis parameters

The behavior of the different components is specified by (1) the contact element, (2) the constraints and degrees of freedom for the components, (3) the applied loads, and (4) the time frame of the simulation. The contact element used in the analysis was called automatic surface to surface for the two pairs of contacting components: one for the top compression plate and the substrate, and the other for the bottom plate and the substrate. In addition, force transducers were added to the top compression plate to measure and export the reaction forces of the simulation. The bottom compression plate was rigidly constrained in all three translational and rotational axes. The top plate was constrained in two axes for translational and all three rotational axes, allowing only one degree of freedom to simulate the vertical movement of the cross-head of a mechanical tester. The substrate was constrained in both axes in the plane of the compression plates to prevent any translational motion. The load was applied by the top plate and was simulated in the model by using a boundary prescribed motion rigid element, which was moving at a constant velocity of 1 mm/min to mimic the strain rate used for compression testing. The termination time was defined as the time required to fully compress the substrate or the time when a maximum force of 5 kN was applied while the time interval between measurements was set to 1 sec for better accuracy with the empirical data.

### Results from FEM

Figure 11 compared the stress-strain curves generated by the model with the experimental data. The curves demonstrate the linear elastic region, which was where the elastic modulus values were measured. Table I displayed the elastic modulus values found from both the model and experimental data.

**TABLE I**
**Comparison of Simulated and Actual Modulus Values of the Porous Substrates**

| Salt-to-polymer mass ratio | Simulated modulus (MPa) | Empirical modulus (MPa) | Percent error (%) |
|---|---|---|---|
| 3 | 15.68 | 15.77 | 0.57 |
| 6 | 4.24 | 4.65 | 8.82 |
| 9 | 2.94 | 2.88 | 2.08 |

The comparison showed that the approximated and empirical values corresponded well with respect to each other with reasonable percent errors. The good agreement between the experimental data and modeling results suggest that relative density was the main contributor to the mechanical properties as the model did not consider some of the other physical properties such as pore size, pore density, and open porosity content. However, it can be speculated that parameters, such as pore size and pore density could not have significantly contributed to the mechanical properties because their trends cancelled each other out due to the varying pore wall thickness, as discussed earlier. On the other hand, although open porosity content was not considered in the model, it is inversely proportional to the relative density, which agrees with its trend with mechanical properties. Thus, the experimental data for open porosity would reinforce the modeling results. Therefore, the good agreement between the experimental data and modeling results can be predominately attributed to the relative density of the porous substrate.

## CONCLUSIONS

Novel open-porous conductive PPy-PLA composites were successfully fabricated using compression molding and salt leaching techniques with *in situ* polymerization of PPy. It was found that with increasing salt content, the relative density and elastic modulus decreased while the open porosity and conductivity increased. The pore size and pore density remained independent of salt content. The pore size was controlled by the size of the incorporated salt particles that were eventually leached out. The effect of coating the porous substrates with PPy was negligible when varying the salt content except for the composites fabricated with the salt-to-polymer mass ratio of 3. These coated composites generated elastic modulus values that were more than twice the uncoated samples for the same relative density, because of the stiffening effects of the pore walls. Development of a finite element model for compression testing of the open-porous substrates demonstrated an agreeable correlation with the experimental results. These results provide the basis for the extended development and characterization of the novel porous composites.

## References


1. Truong, V. T.; Codd, A. R.; Forsyth, M. J Mater Sci 1994, 29, 4331.
2. Scher, H.; Zallen, R. J. Chem Phys 1970, 53, 3759.
3. De Jesus, M. C.; Fu, Y.; Weiss, R. A. Polym Eng Sci 1997, 37, 1936.
4. Nicolau, Y. F.; Davied, S.; Genoud, F.; Nechtschein, M.; Travers, J. P. Synth Met 1991, 42, 1491.
5. Bjorklund, R. B.; Lundstrom, I. J Electron Mater 1984, 13, 211.
6. Castilloortega, M. M.; Inoue, M. B.; Inoue, M. Synth Met 1989, 28, C65.
7. Chen, X.; Devaux, J.; Issi, J.; Billaud, D. Polym Eng Sci 1995, 35, 642.
8. Hwang, B. J.; Lee, K. L. Thin Solid Films 1995, 254, 23.
9. Pini, N.; Siegrist, M.; Busato, S.; Ermanni, P. Polym Eng Sci 2007, 47, 662.
10. Nakata, M.; Kise, H. Polym 1993, 25, 91.
11. Pron, A.; Zagorska, M.; Fabianowski, W.; Raynor, J. B.; Lefrant, S. Polym Commun 1987, 28, 193.
12. Wang, Y.; Sotzing, G. A.; Weiss, R. A. Chem Mat 2008, 20, 2574.
13. Sahoo, N. G.; Jung, Y. C.; Goo, N. S.; Cho, J. W. Macromol Mater Eng 2005, 290, 1049.
14. Heino, A.; Naukkarinen, A.; Kulju, T.; Tormala, P.; Pohjonen, T.; Makela, E. A. J Biomed Mater Res 1996, 30, 187.
15. Auras, R.; Harte, B.; Selke, S. Macromol Biosci 2004, 4, 835.
16. Ruckenstein, E.; Chen, J. J Appl Polym Sci 1991, 43, 1209.
17. Ruckenstein, E.; Park, J. S. J Appl Polym Sci 1991, 42, 925.
18. Mikos, A. G.; Thorsen, A. J.; Czerwonka, L. A.; Bao, Y.; Langer, R.; Winslow, D. N.; Vacanti, J. P. Polym J 1994, 35, 1068.
19. Widmer, M. S.; Gupta, P. K.; Lu, L.; Meszlenyi, R. K.; Evans, G. R. D.; Brandt, K.; Savel, T.; Gurlek, A.; Patrick, C. W., Jr.; Mikos, A. G. Biomaterials 1998, 19, 1945.
20. Lee, S.; Kim, B.; Kim, S. H.; Kang, S. W.; Kim, Y. H. Macromol Biosci 2004, 4, 802.
21. Thomson, R. C.; Yaszemski, M. J.; Powers, J. M.; Mikos, A. G. J Biomater Sci Polym Ed 1995, 7, 23.
22. Thomson, R. C.; Yaszemski, M. J.; Powers, J. M.; Mikos, A. G. Biomaterials 1998, 19, 1935.
23. Wu, L.; Ding, J. Biomaterials 2004, 25, 5821.
24. Hou, Q.; Grijpma, D. W.; Feijen, J. Biomaterials 2003, 24, 1937.
25. Ghosh, S.; Gutierrez, V.; Fernández, C.; Rodriguez-Perez, M. A.; Viana, J. C.; Reis, R. L.; Mano, J. F. Acta Biomater 2008, 4, 950.
26. Ashrafi, A.; Golozar, M. A.; Mallakpour, S. Synth Met 2006, 156, 1280.
27. Balci, N.; Akbulut, U.; Toppare, L.; Stanke, D.; Hallensleben, M. L. Tr J Chem 1998, 22, 73.
28. Otero, T. F.; Ariza, M. J. J Phys Chem B 2003, 107, 13954.
29. Omastová, M.; Trchová, M.; Kovářová, J.; Stejskal, J. Synth Met 2003, 138, 447.
30. Babu, K. F.; Senthilkumar, R.; Noel, M.; Kulandainathan, M. A. Synth Met 2009, 159, 1353.
31. Vishnuvardhan, T. K.; Kulkarni, V. R.; Basavaraja, C.; Raghavendra, S. C. Bull Mater Sci 2006, 29, 77.